NUCL SCI TECH (2020) 31:111
https://doi.org/10.1007/s41365-020-00818-2

In vivo SPECT imaging of an ^{131}I-labeled PM 2.5 mimic substitute

Dong-Hui Pan[1,2] · Jie Sheng[2] · Xin-Yu Wang[2] · Qian-Huan Huang[2] · Jun-Jie Yan[2] · Li-Zhen Wang[2] · Run-Ling Yang[2] · Dong-Jian Shi[1] · Yu-Ping Xu[2] · Ming-Qing Chen[1]

Received: 24 May 2020 / Revised: 23 September 2020 / Accepted: 24 September 2020 / Published online: 10 November 2020
© China Science Publishing & Media Ltd. (Science Press), Shanghai Institute of Applied Physics, the Chinese Academy of Sciences, Chinese Nuclear Society and Springer Nature Singapore Pte Ltd. 2020

Abstract The health effects of ambient PM 2.5 and its potential mechanisms have generated considerable interest. In vitro cell studies and ex vivo animal experiments may not accurately determine the characteristics of PM 2.5 particles. To better understand their detailed mechanisms, we performed an in vivo study using single photon emission tomography (SPECT) imaging. To mimic the PM 2.5 particles, SiO_2 nanoparticles modified by ethylene carbonate or polyvinyl pyrrolidone were labeled with ^{131}I. After administration via inhalation, in vivo SPECT imaging of the radiolabeled particles in sprague dawley rats was performed. It was found that radioactivity accumulated in the lungs and trachea 6 and 24 h after administration. In addition, significant radioactivity was observed in the abdomen, including the liver and kidneys. The results were also confirmed by ex vivo autoradiography. This study revealed that in vivo SPECT imaging could be an effective method for investigating the properties of PM 2.5 particles.

Keywords PM 2.5 mimic substitute · EC/SiO_2 nanoparticles · SPECT images · ^{131}I labeling

1 Introduction

Air pollution has aroused widespread public health concerns in China with the rapid growth of the economy and industry. According to the global health observatory data from the WHO, almost 7 million people are killed by air pollution every year [1, 2]. Among them, particulates with aerodynamic diameters of less than 2.5 μm (PM 2.5), which comprise an air-suspended mixture of solid and liquid particles, have become the most criticized pollutant, attracting considerable attention. These particulates can penetrate human lungs and cause many adverse health effects, such as asthma, pneumonia, stroke, chronic bronchitis, and arrhythmia [3–5]. In addition, exposure to a polluted atmosphere for a prolonged period of time is associated with a high incidence of stroke and impaired cognitive function [6]. When the level of PM 2.5 increases by 10 $\mu g/m^3$ in one day from standard levels, hospital admissions for respiratory disease increase by 4–14% [7–9]. It is estimated that the contribution of air pollution to premature mortality might double by 2050 [10].

To date, various studies concerning the effects of PM 2.5 on health have been conducted. For example, PM 2.5 may contribute to systemic oxidative stress and damage mammalian cells, which is considered an essential molecular mechanism of PM 2.5-mediated toxicity [11, 12]. Numerous organic chemicals coated on PM 2.5 can

This work was supported by the National Natural Science Foundation of China (Nos. 31671035, 51803082), National Significant New Drugs Creation Program (No. 2017ZX09304021), Jiangsu Province Foundation (Nos. BK20170204, BK20161137), and Jiangsu Provincial Medical Innovation Team (Nos. CXTDA2017024, LGY2017088, QNRC2016628).

✉ Yu-Ping Xu
xuyuping@jsinm.org

✉ Ming-Qing Chen
mqchen@jiangnan.edu.cn

[1] Key Laboratory of Synthetic and Biological Colloids, School of Chemical and Material Engineering, Ministry of Education, Jiangnan University, Wuxi 214122, China

[2] Key Laboratory of Nuclear Medicine, Jiangsu Key Laboratory of Molecular Nuclear Medicine, Ministry of Health, Jiangsu Institute of Nuclear Medicine, Wuxi 214063, China

produce or increase levels of intracellular reactive oxygen species, which have been identified as signaling molecules in various pathways regulating cell survival and death [13, 14]. In addition, PM 2.5 alters the expression of antioxidant enzymes, including superoxide dismutase and catalase, and decreases their activities [15, 16]. PM 2.5 may also lead to global DNA hypomethylation, P16 gene promoter hypermethylation, and decreased DNA methyltransferase activity in normal subjects as well as notably chronic obstructive pulmonary diseased cells [17–20]. The presence of PM 2.5 can also cause local and systemic inflammation [21–23]. Although these findings from in vitro cell and ex vivo animal experiments are encouraging, there remains a lack of a strategy for systematically and comprehensively evaluating the in vivo behaviors of the particles. To better protect ourselves from PM 2.5, its characteristics, such as biodistribution, metabolic activation, excretion, toxicity, and cellular responses, need to be better understood.

Molecular imaging technology is a growing biomedical research discipline that enables the visualization of physiological or pathological processes in living subjects as well as the quantification of biological processes at the cellular level [24, 25]. Compared with traditional ex vivo studies, molecular imaging allows numerous in vivo experiments to occur repeatedly in the same animal, which markedly reduces costs and shortens the length of time of the experiments. Due to low instrumentation and radionuclide costs, single photon emission tomography (SPECT) is widely used clinically for noninvasive particle detection [26, 27].

Radiohalogen ^{131}I is a theranostic radioactive isotope used in nuclear medicine [28, 29]. For example, ^{131}I-labeled metaiodobenzylguanidine has been applied in the treatment of neuroendocrine tumors. As well as therapy, radioiodine can be used for SPECT imaging by emitting high-energy gamma radiation with more extended half-life periods ($T_{1/2}$ = 8.3 days). Radioiodine is commercially available in China [15]. Due to its complex composition, it is difficult to label neutral PM 2.5 particles with ^{131}I. However, the particles are easy to assemble because of their low surface hydrophobicity. SiO_2 particles are a reasonable substitute because their diameter is similar to that of PM 2.5 [30]. In addition, the interior hollow porous (approximately 5 nm aperture) section is convenient for the adsorption of nuclides. To avoid accumulation, the SiO_2 particles are modified with polyvinyl pyrrolidone (PVP) or ethyl cellulose (EC). PVP is a water-soluble macromolecule commonly used in pharmaceutics. Coating PVP on the surface of SiO_2 particles is beneficial for increasing the hydrophilicity and dispersion of the particles. EC is another water-insoluble but ethanol-soluble polymer commonly used in pharmaceutical preparations. To better evaluate the in vivo properties, the modified SiO_2 nanoparticles were labeled with ^{131}I. After administration of radiolabeled particles to rodents via inhalation, the performance of the radiolabeled compounds, including biodistribution, retention, and metabolism, was determined using SPECT imaging. A schematic illustration of the process is provided in Fig. 1.

2 Methods and materials

2.1 Materials

All commercial reagents were of analytical grade. Sprague dawley (SD) rats were purchased from the Shanghai Laboratory Animal Co. (SLAC), Ltd., China. The ^{131}I sodium iodide solution was obtained from the Chengdu Gaotong Isotope Corporation (China Nuclear Group). Dialysis bags (Amicon centrifugal filter device, MWCO = 30 kDa) were purchased from Merck Millipore, Germany. Phosphate-buffered saline (PBS) was obtained from Sangon Biotechnology (Shanghai, China). PVP and EC were purchased from Sigma-Aldrich. SiO_2 nanoparticles were gifted from China Pharmaceutical University. All reagents were used without further purification.

2.2 Modified SiO_2 nanoparticles with polyvinyl pyrrolidone (PVP/SiO_2)

The SiO_2 nanoparticles modified with PVP (PVP/SiO_2) were prepared according to a previously reported procedure [31]. In brief, 100 mg PVP in 2.5 mL ethanol was mixed with SiO_2 nanoparticles (200 mg) at 25 °C for 2 h. Then, the mixtures were dried at 140 °C to remove residual ethanol. After milling with a pneumatic cracker, PVP/SiO_2 nanoparticles were obtained. The morphological characteristics of the products were determined by scanning electron microscopy (SEM) and dynamic light scattering (DLS).

2.3 Modified SiO_2 nanoparticles with ethyl cellulose (EC/SiO_2)

To prepare EC/SiO_2, ethylene carbonate (500 mg) and SiO_2 nanoparticles (200 mg) were mixed at room temperature for 2 h in the presence of 2 mL ethanol. Then, the mixtures were dried at 140 °C to remove residual ethanol. After milling with a pneumatic cracker, EC/SiO_2 nanoparticles were obtained. The morphological characteristics of the products were determined by SEM and DLS.

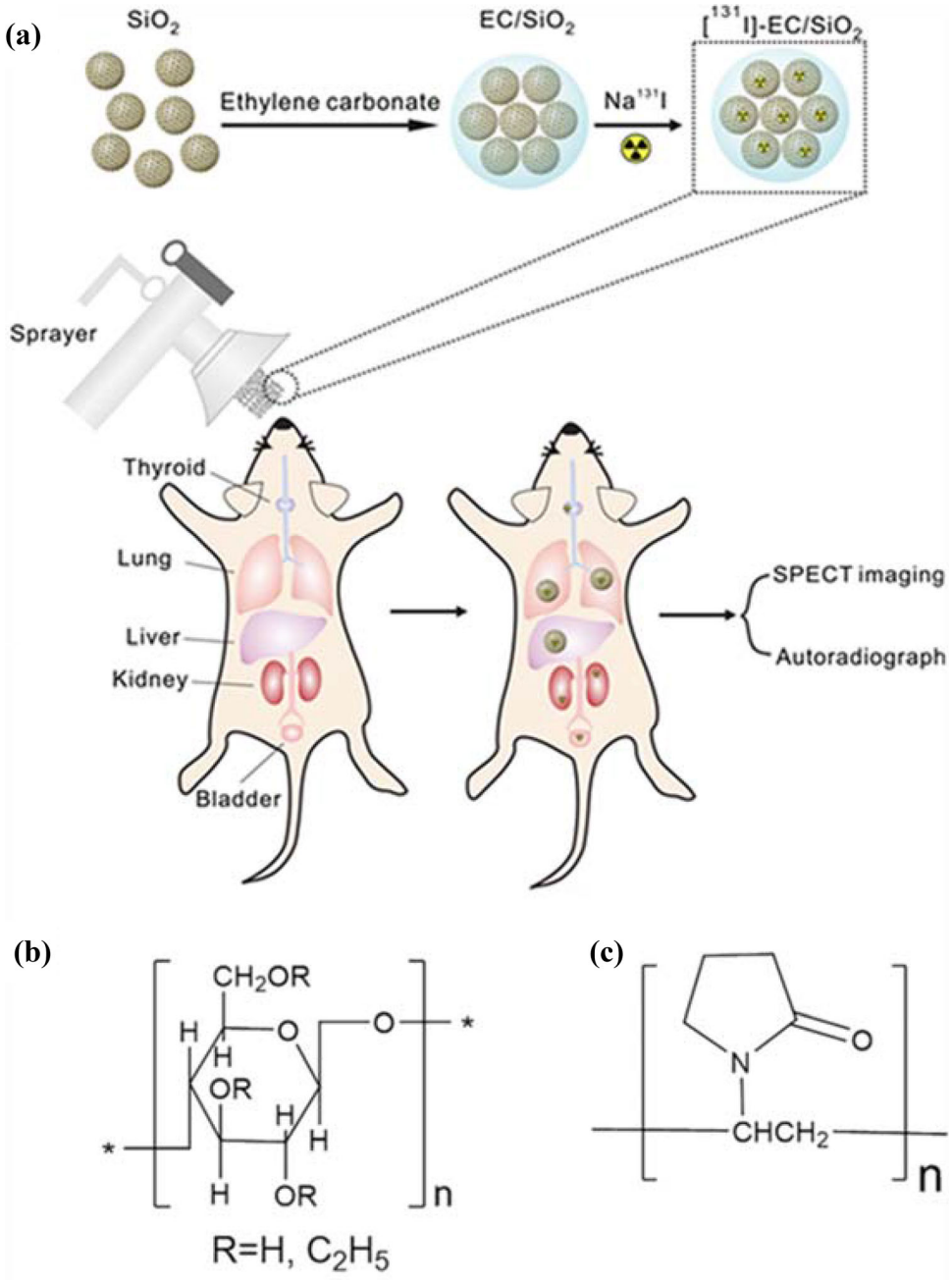

Fig. 1 **a** Schematic illustration of the preparation, administration, and tracking process of [^{131}I]-EC/SiO_2. Chemical structure of **b** EC and **c** PVP

2.4 Preparation of [^{131}I]-EC/SiO_2 nanoparticles

A 2 mL $Na^{131}I$ (3700 MBq) solution was mixed with 500 mg of EC/SiO_2 nanoparticles in 1 mL of ethanol and 1 mL water at room temperature for 240 h. The resulting complexes were then placed in dialysis tubing and dialyzed in deionized water, which was replaced with fresh water every 24 h. The radioactivity in the dialysis bag was monitored using a radioactivity meter (CAPINTEC. INC CRC-25). After removing free ^{131}I, [^{131}I]-EC/SiO_2 nanoparticles were obtained by evaporating the solvents in a vacuum drying oven (DZF-6053 YiHeng, Shanghai) at 50 °C.

2.5 In vitro stability of [^{131}I]-EC/SiO_2 nanoparticles

The in vitro stability of ^{131}I-labeled EC/SiO_2 particles was determined by incubating the radiolabeled compound in PBS and human plasma at 37 °C. The purified [^{131}I]-EC/SiO_2 (200 μL, 3.7 MBq, 0.5 mg, respectively) was placed in a dialysis bag (MWCO = 10 K) and then suspended in 20 mL of plasma or PBS with magnetic stirring. At the selected time intervals (2, 4, 8, 12, and 24 h), 0.5 mL

dialyzate was removed to calculate the radioactivity using a PerkinElmer 1470 γ-counter.

2.6 Inhalation administration

All animal procedures were conducted in accordance with the Guidelines for the Care and Use of Laboratory Animals of the Ministry of Science and Technology of the People's Republic of China's requirements. The Animal Study Committee of the Jiangsu Institute of Nuclear Medicine approved the experiments. The rats were routinely screened for common rat pathogens and housed in specific pathogen-free facilities under standard conditions (24 ± 2 °C, 50 ± 5% humidity) with a 12 h light/dark cycle and food and water available ad libitum.

To ensure the best image quality from SPECT, the [^{131}I]-EC/SiO_2 particles were administrated using a non-surgical intratracheal installation method [32]. Briefly, 5 SD rats (SLAC Laboratory Animal Co., Ltd, China; 6–8 weeks old, 200–300 g) were anesthetized via an intraperitoneal injection of pentobarbital. A small animal laryngoscope was used throughout the process. A ball-tipped needle was maneuvered through the epiglottis, after which contact with the tracheal rings provided confirmation that the needle was inside the trachea. Then, an injector containing 0.2 mL of [^{131}I]-EC/SiO_2 (111 ± 18.5 MBq) was inserted into the ball tripped needle. After gently instilling the substance into the trachea, the animal was maintained in an upright position for 2 min to allow the fluid to drain into the respiratory tree.

2.7 SPECT imaging

After administration via inhalation, the rats were placed in a prone position using a handmade holding device under anesthetization. SPECT imaging was performed at 6 and 24 h post-administration using a Philips Skylight SPECT fitted with a high-energy pinhole collimator [33]. Static images (10 min) of the animals were obtained with a 256 × 256 matrix and 16 bits pixel depth. After imaging, the SPECT data were reconstructed using an ordered-subset expectation maximization algorithm.

Semiquantitative assessment was performed by calculating the target-to-background ratio (TBR). The lungs, liver, and kidneys were considered the target areas, and the blood pool was considered the background area.

2.8 Ex vivo autoradiograph

After SPECT imaging, rats were euthanized with excessive amounts of isoflurane and dissected. The lungs were sectioned, and the slices were laid on X-film in a darkroom and imaged on a Cyclone Plus Storage Phosphor system (PerkinElmer, USA). Region of interest analysis of ex vivo images was carried out to compare uptake in the lobus, lobus medius, and lobus inferior. Quantitative [^{131}I]-EC/SiO_2 uptake was determined by gamma counting of 2 serially sectioned lung tissue specimens.

2.9 Postmortem examinations

For hematoxylin and eosin (HE) staining, the rats were euthanized after SPECT imaging and their tissues, including heart, liver, spleen, kidneys, and lungs, were harvested and fixed in 4% formalin solution at room temperature for 48 h. The tissues were then embedded in paraffin blocks and sectioned into slices with a thickness of 4 μm. The tissue sections were then mounted onto glass slides and stained with HE. The stained sections were examined using an optical microscope.

2.10 Statistical analysis

Statistical analyses were performed using GraphPad Prism software. Data were analyzed using the unpaired, two-tailed Student's t-test. Differences at the 95% confidence level ($p < 0.05$) were considered statistically significant.

3 Results and discussion

3.1 Characterization of modified SiO_2 nanoparticles

As shown in Fig. 2, the average size of the unmodified SiO_2 particles was approximately 3.5 μm. Both the PVP/SiO_2 and EC/SiO_2 nanoparticles were well dispersed in water. DLS showed that the uniform sizes of PVP/SiO_2 and EC/SiO_2 nanoparticles were approximately 3 and 1.2 μm, respectively (Fig. 2). The findings of DLS and SEM revealed that both PVP/SiO_2 and EC/SiO_2 nanoparticles possessed spherical shapes with diameters of nearly 3 and 1.2 μm, respectively (Fig. 2). Since the diameter was larger than 2.5 μm, PVP/SiO_2 particles may not be applicable for the following studies.

In addition, considering the water solubility of PVP, PVP/SiO_2 nanoparticles may be unstable in vivo. On the contrary, EC/SiO_2 nanoparticles can be applied to mimic PM 2.5 particles because EC has been widely used in biomedicine and life sciences.

3.2 Preparation of ^{131}I-labeled EC/SiO_2 nanoparticles

The EC/SiO_2 nanoparticles were further labeled with ^{131}I to investigate the characteristics of PM 2.5 particles.

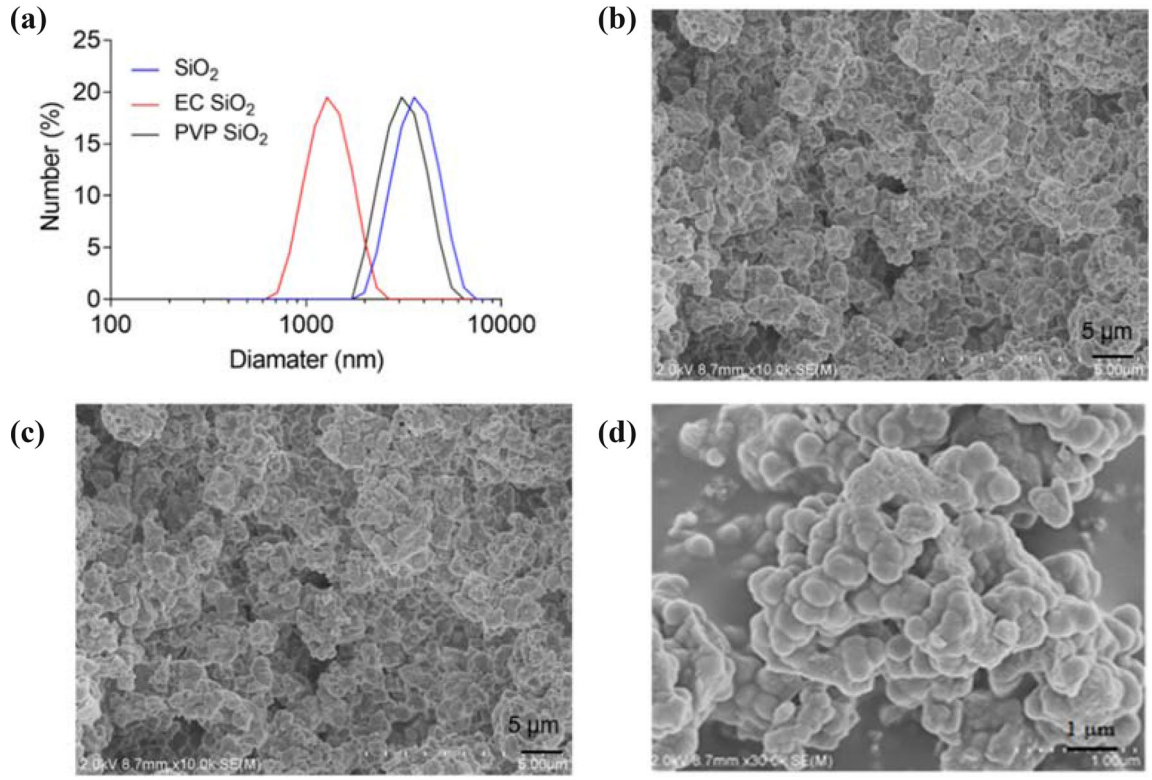

Fig. 2 **a** Size distribution of SiO_2, EC/SiO_2, and PVP/SiO_2 in water determined by DLS. SEM images of **b** SiO_2, **c** PVP/SiO_2, and **d** EC/SiO_2

To determine whether the diameter of the [^{131}I]-EC/SiO_2 nanoparticles met the requirements to mimic PM 2.5 for the in vivo study, non-radioactive iodine was first adsorbed on EC/SiO_2 nanoparticles. The particle size was found to be smaller than 2.5 μm (Fig. 3a). After radiolabeling with ^{131}I, the radiolabeling yield and stability were measured. The labeling yield gradually decreased because of the dissociation of free ^{131}I from the ^{131}I-EC/SiO_2 nanoparticles. After dialyzing for 168 h, the labeling yields of [^{131}I]-EC/SiO_2 nanoparticles remained constant (~ 30%), and no further free ^{131}I was found outside the dialysis bag (Fig. 3b). This indicated that ^{131}I was successfully labeled in the EC/SiO_2 nanoparticles. Less than 3% ^{131}I was released from the [^{131}I]-EC/SiO_2 after 24 h of incubation in PBS or serum (Fig. 3c). This implied that ^{131}I can be easily labeled on the EC/SiO_2 nanoparticles, and [^{131}I]-EC/SiO_2 nanoparticles exhibit high radiostability in vitro, indicating that the particles could be further applied to tracing PM 2.5 in vivo.

3.3 Inhalation and in vivo SPECT imaging

We analyzed the characteristics of PM 2.5 via molecular imaging. The in vivo biodistribution of [^{131}I]-EC/SiO_2 nanoparticles, the "mimic PM 2.5," was further investigated. The [^{131}I]-EC/SiO_2 nanoparticles were administered

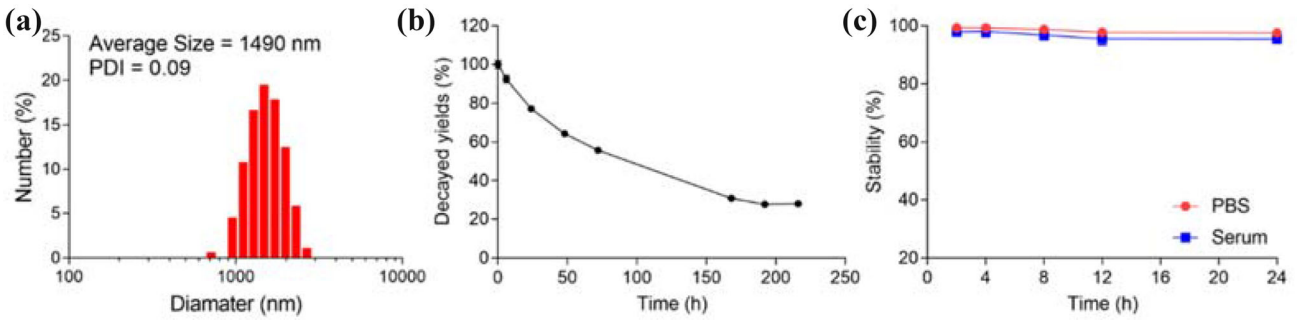

Fig. 3 **a** Size distribution of EC/SiO_2-I in water determined by DLS. **b** Decayed yields of [^{131}I]-EC/SiO_2 over time. **c** In vitro stability of [^{131}I]-EC/SiO_2 particles incubated in PBS solution and serum

to the rats (n = 5) by endotracheal intubation. The inhaled radio dose of [^{131}I]-EC/SiO_2 was 111 ± 18.5 MBq, with a total mass of 300 mg.

SPECT imaging was performed at 6 and 24 h post-administration. After 6 h of administration, SPECT images showed that the TBR of the lungs was 11.85 ± 3.90 (Fig. 4). At the same time, the TBRs of the liver, kidneys, and bladder were 7.27 ± 0.72, 2.56 ± 0.24, and 0.76 ± 0.05, respectively. After 24 h of administration, the TBRs of the lungs and bladder were 2.33 ± 0.86 and 5.33 ± 1.63, respectively.

In vivo SPECT imaging showed that the radiotracer was mainly located in the lungs, which was in accordance with the finding that the lungs are the target organ of PM 2.5 [18, 21, 30]. Radioactivity was also identified in other healthy organs, such as the heart, kidneys, and liver. It appears that PM 2.5 could penetrate human body tissue. Delayed images at 24 h post-administration showed that the particles were mostly eliminated from the urinary passage. Moreover, moderate radio signals appeared in the abdomen, especially in the intestine. This implies that particles might also be excreted via feces.

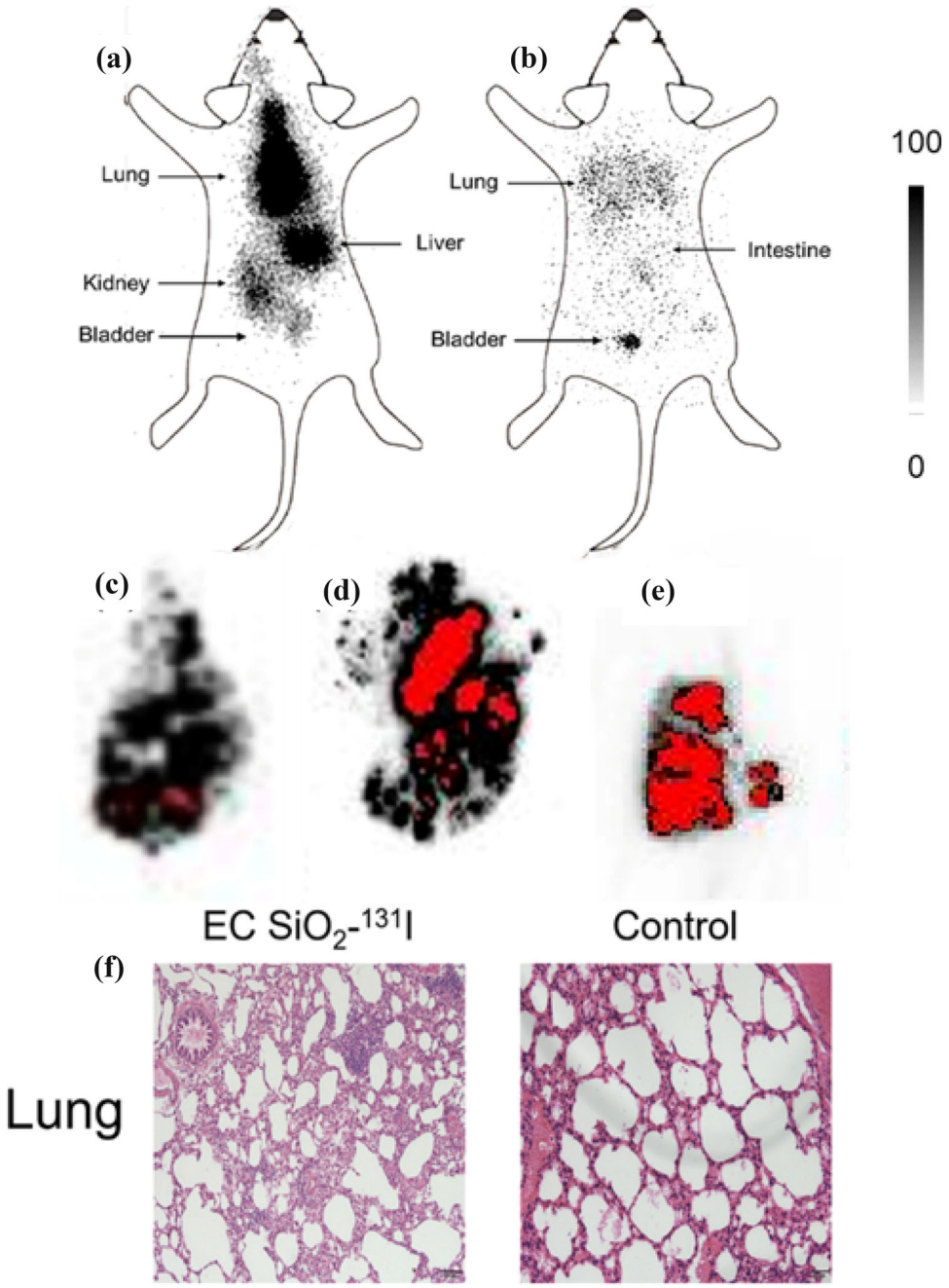

Fig. 4 SPECT images of [^{131}I]-EC/SiO_2 in rats at 6 **a** and 24 h **b** post-administration. Ex vivo autoradiograph of rat lungs **c**, **d** outside fields of the lungs, and **e** inside fields of lungs at 24 h post-administration. **f** HE-stained lung section at 24 h post-administration

Molecular imaging technology, including PET and SPECT, has been widely used clinically for tumor diagnosis, cancer staging, and therapeutic response monitoring. This is the first time, to our knowledge, that molecular imaging technology has been used for the visualization of PM 2.5 particles in vivo. Image-based quantitation of PM 2.5 generated by SPECT also enabled real-time noninvasive data analysis. This study provides accurate measurements of PM 2.5.

However, limitations of this study still exist. The association between the adverse effects of air pollution and cardiovascular and respiratory health as well as cognitive functioning has been well documented [7, 34, 35], but this study did not investigate these features. In addition, air pollution is multifaceted, as it comprises numerous environmental toxins [31]. However, in the present study, the mimic PM 2.5 particles were composed of only one component. Meanwhile, the long-term effects were not evaluated. In addition, the thyroid of the SD rats was not blocked, which resulted in mild uptakes into the thyroid. All these challenges will be solved in future with further research.

3.4 In vivo autoradiograph and HE staining

To verify the SPECT results, ex vivo autoradiography and HE staining were conducted. After SPECT imaging, rats were euthanized and autoradiographs were performed. Exposure to the phosphor imaging plates for 12 h provided a favorable autoradiographic signal-to-noise ratio. It was found that a higher density of radioactivity was distributed in the inside fields of the lungs (red areas) (Fig. 4e) than in the outside fields of the lungs (black areas) (Figs. 4c, d). Particles were primarily localized in the trachea (red areas; Figs. 4c, d, e), which was consistent with the results of SPECT imaging.

Briefly, for HE staining, the lung tissues of [^{131}I]-EC/SiO_2-inhaled rats and normal rats were collected, sliced, and stained with HE to assess the PM 2.5-induced injury. The lung tissues of the normal rats exhibited an intact structure (Fig. 4f). The alveolar space was bright, and there was no edema in the alveolar septum. However, increased exudates, congestion in the pulmonary alveolus, and collapse, rupture, and fusion of the pulmonary alveoli were observed in the lung tissues of the [^{131}I]-EC/SiO_2-inhaled rats. Compared with the normal group, the thickness of the alveolar septum significantly increased. PM 2.5 particles may cause serious lung injury.

4 Conclusion

In summary, we successfully developed a novel molecular imaging measurement method for PM 2.5 distribution and metabolism detection in SD rats. EC and PVP were used to screen for the most favorable substitute. EC/SiO_2 exhibited a smaller size and a uniform spherical shape. EC/SiO_2 not only possesses the appropriate particle size but can also be successfully labeled on 131I with high stability. SPECT imaging showed the biodistribution of the "mimic PM 2.5" after administration via inhalation. Subsequently, the autoradiograph and HE-stained images were consistent with SPECT imaging results. Therefore, we conclude that this molecular imaging method could be a novel and effective technique for the detection and visualization of PM 2.5 metabolism. The preclinical studies were satisfactory, and further studies are currently being undertaken.

References

1. G.H. Yang, Y. Wang, Y.X. Zeng et al., Rapid health transition in China, 1990–2010: findings from the global burden of disease study 2010. Lancet (London, England) **381**(9882), 1987–2015 (2013). https://doi.org/10.1016/S0140-6736(13)61097-1
2. J. Lelieveld, J.S. Evans, M. Fanis et al., The contribution of outdoor air pollution sources to premature mortality on a global scale. Nat. **525**(7569), 367–371 (2015). https://doi.org/10.1038/nature15371
3. H.B. Guo, S.J. Huang, M.X. Chen et al., Air pollutants and asthma patient visits: Indication of source influence. Sci. Total Environ. **625**, 355–362 (2018). https://doi.org/10.1016/j.scitotenv.2017.12.298
4. V.C. Pan, F. Kazemiparkouhi, J. Manjourides et al., Long-term PM 2.5 exposures and respiratory, cancer and cardiovascular mortality in american older adults. Am. J. Epidemiol. **186**(8), 961–969 (2017)
5. Q. Wang, J.N. Wang, M.Z. Zeng et al., A county-level estimate of PM 2.5 related chronic mortality risk in China based on multi-model exposure data. Environ. Int. **110**, 105–112 (2017)
6. E.H. Wilker, S.R. Preis, A.S. Beiser et al., Long-term exposure to fine particulate matter, residential proximity to major roads and measures of brain structure. Stroke **46**(5), 1161–1166 (2012). https://doi.org/10.1161/STROKEAHA.114.00834
7. A. Zanobetti, J. Schwartz, The effect of fine and coarse particulate air pollution on mortality: a national analysis. Environ. Health Perspect. **117**(6), 898–903 (2009). https://doi.org/10.1289/ehp.0800108
8. M. Franklin, P. Koutrakis, J. Schwartz, The role of particle composition on the association between PM 2.5 and mortality. Epidemiol. **19**(5), 680–689 (2002)
9. K.A. Miller, D.S. Siscovick, L. Sheppard et al., Long-term exposure to air pollution and incidence of cardiovascular events in women. New Engl. J. Med. **356**(5), 447–458 (2007). https://doi.org/10.1016/j.envint.2017.10.015
10. J. Lelieveld, J.S. Evans, M. Fnais et al., The contribution of outdoor air pollution sources to premature mortality on a global

scale. Nat. **525**(7569), 367–371 (2015). https://doi.org/10.1056/NEJMoa054409
11. W. Liu, M. Zhang, J. Feng et al., The influence of quercetin on maternal immunity, oxidative stress, and inflammation in mice with exposure of fine particulate matter during gestation. Int. J. Environ. Res. Public Health **14**(6), 592–607 (2017). https://doi.org/10.3390/ijerph14060592
12. O.G. Aztatzi-Aguilar, M. Uribe-Ramírez, J. Narváez-Zorales et al., Early kidney damage induced by subchronic exposure to PM 2.5 in rats. Part. Fibre Toxicol. **13**(1), 68–87 (2016)
13. Y. Wei, X.N. Cao, X.L. Tang et al., Urban fine particulate matter (PM 2.5) exposure destroys blood-testis barrier (BTB) integrity through excessive ROS-mediated autophagy. Toxicol. Mech. Methods **28**(4), 302–339 (2018)
14. W. Zhou, D.D. Tian, H. Jun et al., Repeated PM 2.5 exposure inhibits BEAS-2B cell P53 expression through ROS-Akt-DNMT3B pathway-mediated promoter hypermethylation. Oncotarget **7**(15), 20691–20703 (2016)
15. B. Crobeddu, L. Aragao-Santiago, L.C. Bui et al., Oxidative potential of particulate matter 2.5 as predictive indicator of cellular stress. Environ. Pollut. **230**, 125–135 (2017)
16. S.L. Feng, D. Gao, F. Liao et al., The health effects of ambient PM 2.5 and potential mechanisms. Ecotoxicol. Environ. Saf. **128**, 67–74 (2016)
17. M. Plusquin, F. Guida, S. Polidoro et al., DNA methylation and exposure to ambient air pollution in two prospective cohorts. Environ. Int. **108**, 127–136 (2017). https://doi.org/10.1016/j.envint.2017.08.006
18. R.J. Chen, X. Meng, A. Zhao et al., DNA hypomethylation and its mediation in the effects of fine particulate air pollution on cardiovascular biomarkers: a randomized crossover trial. Environ. Int. **94**, 614–619 (2016). https://doi.org/10.1016/j.envint.2016.06.026
19. B. Leclercq, A. Platel, S. Antherieu et al., Genetic and epigenetic alterations in normal and sensitive COPD diseased human bronchial epithelial cells repeatedly exposed to air pollution derived PM 2.5. Environ. Pollut. **230**, 163–177 (2017)
20. C.V. Breton, J. Yao, J. Millstein et al., Prenatal air pollution exposures, DNA methyl transferase genotypes, and associations with newborn LINE1 and alu methylation and childhood blood pressure and carotid intima-media thickness in the Children's Health Study. Environ. Health Perspect. **124**(12), 1905–1912 (2016). https://doi.org/10.1289/EHP181
21. B.F. Cachon, S. Firmin, A. Verdin et al., Proinflammatory effects and oxidative stress within human bronchial epithelial cells exposed to atmospheric particulate matter (PM 2.5 and PM >2.5) collected from Cotonou, Benin. Environ. Pollut. **185**, 340–351 (2014)
22. C.W. Liu, T.L. Lee, Y.C. Chen et al., PM 25 induced oxidative stress increases intercellular adhesion molecule-1 expression in lung epithelial cells through the IL-6/AKT/STAT3/NF-kappaB-dependent pathway. Part Fibre Toxicol. **15**(1), 4–19 (2018)
23. T. Ku, B. Li, R. Gao et al., NF-kappaB-regulated microRNA-574-5p underlies synaptic and cognitive impairment in response to atmospheric PM 2.5 aspiration. Part Fibre Toxicol. **14**(1), 34–52 (2017)
24. B. Carney, S. Kossatz, T. Reiner, Molecular imaging of PARP. J. Nucl. Med. **58**(7), 1025–1030 (2017). https://doi.org/10.2967/jnumed.117.189936
25. K.H. Jung, K.H. Lee, Molecular imaging in the era of personalized medicine. J. Pathol. Transl. Med. **49**(1), 43–58 (2013). https://doi.org/10.4132/jptm.2014.10.24
26. B.S. Jang, MicroSPECT and MicroPET imaging of small animals for drug development. Toxicol. Res. **29**(1), 1–6 (2013). https://doi.org/10.5487/TR.2013.29.1.001
27. D.R. Osborne, C. Kuntner, S. Berr et al., Guidance for efficient small animal imaging quality control. Mol. Imaging Biol. **19**(4), 485–498 (2017). https://doi.org/10.1007/s11307-016-1012-3
28. M. D'Huyvetter, J. De Vos, C. Xavier et al., ^{131}I-labeled Anti-HER2 camelid sdAb as a theranostic tool in cancer treatment. Clin. Cancer Res. An Official J. Am. Assoc. Cancer Res. **23**(21), 6616–6628 (2017). https://doi.org/10.1158/1078-0432.CCR-17-0310
29. J. Sheng, X.Y. Wang, J. Yan et al., Theranostic radioiodine-labelled melanin nanoparticles inspired by clinical brachytherapy seeds. J. Mater. Chem. B **6**(48), 8163–8169 (2018). https://doi.org/10.1039/c8tb02817f
30. G.Y. Song, Z.J. Li, K.H. Li et al., SiO2/ZnO composite hollow sub-micron fibers: fabrication from facile single capillary electrospinning and their photoluminescence properties. Nanomater. **7**(3), 53–62 (2017). https://doi.org/10.3390/nano7030053
31. C.S. Thompson, M. Zou, Nanostructured PVP/SiO_2 antireflective coating for solar panel applications. Nanotechnol. IEEE (2013). https://doi.org/10.1109/NANO.2013.6721058
32. G. Hatch, R. Slade, E. Boykin et al., Correlation of effects of inhaled versus intratracheally injected metals on susceptibility to respiratory infection in mice. Am. Rev. Respir. Dis. **124**, 167–173 (1981). https://doi.org/10.1164/arrd.1981.124.2.167
33. Y.K. Dewaraja, M. Ljungberg, A.J. Green et al., MIRD pamphlet No. 24: guidelines for quantitative 131I SPECT in dosimetry applications. J. Nucl. Med. **54**(12), 2182–2188 (2013)
34. J.G. Miller, J.S. Gillette, E.M. Manczak et al., Fine particle air pollution and physiological reactivity to social stress in adolescence: the moderating role of anxiety and depression. Psychosom. Med. **81**(7), 641–648 (2019). https://doi.org/10.1097/PSY.0000000000000714
35. P.L. Ljungman, M.A. Mittleman, Ambient Air Pollution and Stroke. Stroke **45**(12), 3734–3741 (2014). https://doi.org/10.1161/STROKEAHA.114.003130